

Surface vibrations in the T₄ and H₃ Pb phases on Si(111)

Eugen Speiser,^{*} Arne Baumann, Sandhya Chandola, and Norbert Esser

Leibniz-Institut für Analytische Wissenschaften - ISAS - e.V., Schwarzschildstraße 8, 12489 Berlin, Germany

Maedeh Zahedifar and Peter Kratzer

Fakultät für Physik und Center for Nanointegration (CENIDE), Universität Duisburg-Essen, Lotharstraße 1, 47057 Duisburg, Germany

Christoph Tegenkamp

Institut für Festkörperphysik, Leibniz Universität Hannover, Appelstraße 2, 30167 Hannover, Germany

and Institut für Physik, Technische Universität Chemnitz, Reichenhainer Strasse 70, 09126 Chemnitz, Germany

 (Received 9 May 2018; revised manuscript received 7 September 2018; published 19 November 2018)

We present here a combined experimental Raman spectroscopy and *ab initio* theoretical study of the vibrational modes of the $(\sqrt{3} \times \sqrt{3})$ reconstructed SIC phase of Pb on Si(111) and discuss their relation to the atomic surface structure. The Raman response of the surface localized vibrational modes, in particular, is identified in the low-frequency spectral range (down to 15 cm^{-1}). We demonstrate that Raman spectroscopy is a very powerful approach to test atomic structures of surfaces and a valuable complement to standard surface analytics. While the calculated spectra of H₃ and T₄ are too similar to allow a discrimination of these phases, the good overall agreement to the measured Raman spectra enables a classification of the observed vibrational modes.

DOI: [10.1103/PhysRevB.98.195427](https://doi.org/10.1103/PhysRevB.98.195427)

I. INTRODUCTION

Metallic adlayers on semiconducting templates provide a superb playground to study intriguing electronic phenomena in low-dimensional systems, e.g., spin density waves or Peierls-driven metal insulator transitions [1]. Among other examples the Pb/Si(111) system has triggered intense research over the last two decades, since the immiscibility of both elements guarantees atomically sharp interfaces [2]. Moreover, a recent theoretical study has demonstrated the effect of Pb layer thickness on the phonon band structure and the electron-phonon coupling [3]. Pb/Si(111) is an excellent system to prepare 2D quantum films [4] as well as various 2D and quasi-2D electron gases with tunable chemical potentials [5]. These layers are electronically well decoupled from the substrate and reveal a 1D transport regime if grown as 2D ribbons on vicinal templates [6]. This has opened the possibility to study growth modes triggered by quantum well states [4], spin-orbit induced Rashba-splitting [7,8] and proximity effects of superconducting states of Pb islands [9].

Moreover, for 2D Pb monolayer phases, such as the densely packed so-called striped incommensurate (SIC) phase on Si(111), superconductivity was reported [10,11], revealing the particular importance of electron-phonon coupling. Since for Pb monolayers, superconducting properties are different from those of Pb multilayers (≥ 2 ML), it was suggested that the Pb-Si-interface phonons govern the electron phonon interaction [11].

The wetting layer regime of Pb/Si(111) hosts a wide variety of superstructures, ranging from the chainlike linear phases to hexagonal phases, within the so-called *devil's staircase* regime from 1.20–1.33 ML [5,12–14]. These superstructures are generated by two structural motifs: the $(\sqrt{7} \times \sqrt{3})$ unit cell and the $(\sqrt{3} \times \sqrt{3})$ unit cell referring to coverages of 6/5 ML and 4/3 ML, respectively [5,12]. The elucidation of the atomic structure of the unit cells has drawn a large amount of attention in the last few decades [13,15–17].

For the $(\sqrt{3} \times \sqrt{3})$ reconstructions two distinct local structures (H₃ and T₄) are proposed (Fig. 1). According to DFT calculations the total energies of the two structures differ by less than 0.01 eV per (1×1) unit cell [14,18]. This may result in the formation of superstructures with different coexisting local structures. The SIC phase is such a superstructure being most likely composed of H₃ and T₄ domains [5]. However, an experimental proof of surface structure details, in particular on multidomain surfaces, remains difficult; only small differences for the T₄ and H₃ models appear in simulated scanning tunneling microscopy images [14].

This paper focuses on the surface vibrational properties and the correlation of surface vibrational eigenmodes to the atomic structure of the Pb/Si(111) $(\sqrt{3} \times \sqrt{3})$ reconstructed SIC phase. We investigate the monolayer structure by surface Raman spectroscopy (SRS) revealing the surface local vibrational properties [19,20], which are, similar to fingerprint spectra of molecules, uniquely linked to the local structure and chemical bonding. By combining SRS with DFT based slab calculations it is possible to attribute the observed Raman lines to surface phonon eigenmodes, thus establishing a direct link to the surface atomic structure [20–22]. To this end we calculate the eigenfrequencies, displacement patterns,

^{*}eugen.speiser@isas.de

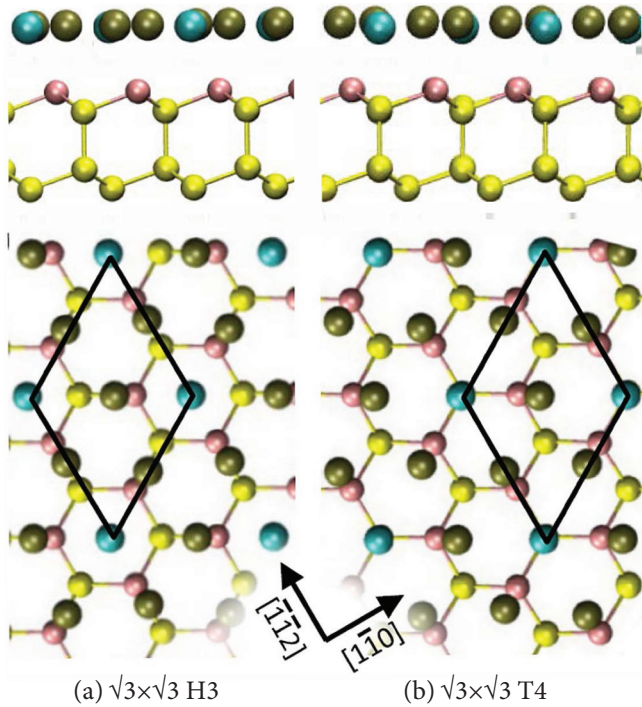


FIG. 1. Side (on top) and top views (bottom) of the structure models for the $(\sqrt{3} \times \sqrt{3})$ reconstructions of Si(111)-Pb [14]. Si substrate atoms are indicated in yellow (second layer) and magenta (first layer). Three Pb atoms (olive) saturate the Si dangling bonds by adsorbing on top of first layer Si atoms (T1, magenta), while one Pb atom (light blue) adsorbs above a second layer Si atom (T4, yellow) or above the hollow site (H3). The respective unit cells are labeled T4 or H3 according to the adsorption site closest to the central Pb atom. The corresponding unit cells (solid rhomboid) are indicated.

and the Raman response of the relevant surface localized eigenmodes.

II. EXPERIMENT

The experiments were performed in ultrahigh vacuum (UHV) (base pressure 2×10^{-10} mbar). Si(111) wafers with n -type doping [resistivity 0.1–20 Ω cm, offset of 1° towards the $(\bar{1}\bar{1}2)$ direction] were used. The reconstructed Si(111) surface was prepared by flash annealing and well-ordered atomic Pb layers (1.20 to 1.33 ML) were grown following the procedure described in Ref. [8]. Low-energy electron diffraction was employed to examine the resulting surface reconstructions [5,12]. Unreconstructed reference surfaces were prepared by subsequent exposure to air at 8×10^{-8} mbar for 30 min in UHV.

Raman spectroscopy was performed in near backscattering configuration at a sample temperature of 50 K. A laser excitation of 1.91 eV (647.1 nm) was chosen in resonant condition to the surface electronic band structure [23]. The spectral resolution of the Raman spectrometer, as verified by plasma lines, was 1.2 cm^{-1} . The experimental accuracy of the spectral lines is determined to $<0.5 \text{ cm}^{-1}$. The Raman spectra were recorded for different polarization configurations, i.e., either parallel or crossed polarizations of incident and scattered light, denoted as $\mathbf{z}(\mathbf{y}\mathbf{y})\bar{\mathbf{z}}$ (A' symmetry) and the $\mathbf{z}(\mathbf{x}\mathbf{y})\bar{\mathbf{z}}$

(A'' symmetry) polarization configurations (Porto notation). Assuming a C_{3v} symmetry of the Pb/Si(111) $(\sqrt{3} \times \sqrt{3})$ structure A' modes are symmetry conserving while A'' are symmetry breaking modes of the individual structures. I.e., Raman modes of any structure with C_{3v} symmetry are either A' or A'' modes. For the Pb/Si(111) structure in the present work however, the C_{3v} symmetry applies only approximately, according to the calculated geometries (see discussion below). Therefore, sharp polarization selection rules may not be expected.

III. FIRST-PRINCIPLES CALCULATIONS

For comparison with experiment, the phonon frequencies and displacement vectors of the Pb modes have been calculated from first principles using density functional theory. We employ the generalized gradient approximation (GGA) exchange-correlation functional [24] and the projector augmented-wave method [25] implemented in the software package VASP [26]. The Si and Pb pseudopotentials include $3s3p$ and $5d6s6p$ electrons as valence electrons, and the wave functions are expanded in a plane-wave basis set up to an energy cutoff of 400 eV. The spin degree of freedom was not considered, and the effect of spin-orbit coupling at the Pb atoms was disregarded. As seen in Ref. [27], the vibrational peak positions undergo only minor shifts when spin-orbit interactions are taken into account. With these settings, the Si lattice constant is obtained as 5.47 \AA , about 0.7% larger than the experimental value.

By modeling separately the T4 and H3 structures, we neglect the possible strain relief in the SIC phase due to the coexistence of different domains. Different from Ref. [23], we use a thicker slab (seven bilayers) to model the Si substrate. Moreover, after relaxation of the atomic positions, the C_{3v} symmetry of the clean Si(111) surface is no longer preserved, since the positions of the T4 atom moved away from the threefold rotational axis. The atomic geometries of the H3 and T4 structures obtained from the calculation are shown in Fig. 1.

From the calculated surface structures (Fig. 1), the force constants, and hence the phonon frequencies and eigenvectors at $\bar{\Gamma}$ for both structures, are obtained using density functional perturbation theory [28]. With the same method, the static dielectric response is calculated, and the tensor $Z_{\alpha\beta}$ of the Born effective charges is extracted for each atom. Each component of this tensor is defined as the first derivative of the Cartesian component P_β of the polarization with respect to the ionic coordinate R_α .

For nonresonant Raman scattering, the Raman tensor can be expressed within Placzek's approximation (see Ref. [29] for a derivation) via the electronic polarizability tensor. The polarizability associated with a specific phonon mode is calculated within the dipole approximation from the Born effective charges of the atoms involved in the displacements. In summary, the Raman intensity is given by [30]

$$I \sim \sum_{\alpha} \left| \sum_l \sum_{\beta} Z_{\alpha\beta} e_{\beta}(l) \right|^2, \quad (1)$$

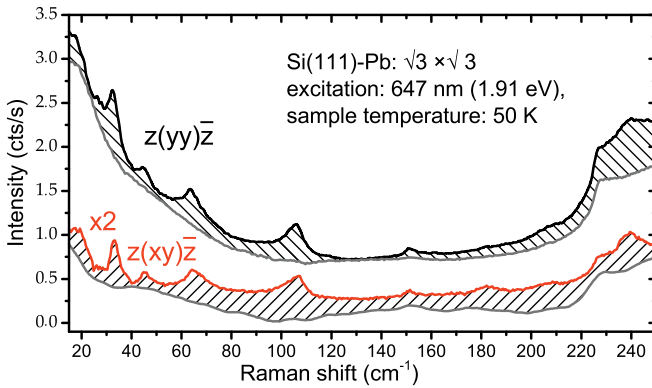


FIG. 2. SRS spectra of the $(\sqrt{3} \times \sqrt{3})$ reconstructed Si(111)-Pb surface and the nonordered reference surface (gray) in parallel and perpendicular polarization configurations $\mathbf{z}(\mathbf{y}\mathbf{y})\bar{\mathbf{z}}$ (A' symmetry) (black) and $\mathbf{z}(\mathbf{x}\mathbf{y})\bar{\mathbf{z}}$ (A'') (red). The intensity difference between reconstructed and reference surface (shaded area) reveals the surface response.

where $\vec{e}_\beta(l)$ is the eigenvector belonging to phonon mode l , $Z_{\alpha\beta}$ is the tensor of the Born effective charges, and the summation indices α and β both run over the Cartesian coordinates of all atoms. Since the electric field vector of the light is lying in the surface plane, only the in-plane components x and y are summed over, i.e., the calculation averages over Raman contributions with A' and A'' symmetry. We would like to note that this theoretical approach to calculate Raman lines will deliver a limited accuracy with respect to the intensities of experimental lines due to the neglect of electronic resonance effects [19,31].

For the assignment of modes, the displacement patterns for the T4 structure reported in Ref. [23] are very useful, since they allow us to classify the displacement patterns into five classes (see Chap. IV). Despite minor differences, this classification is valid both for the present results as well as for the previous results on the T4 [23] and H3 [27] structures. Compared to the phonons in bulk Pb, the optical phonons of the Pb/Si(111) surface are found at significantly higher energies, owing to the direction-dependent interaction between the Pb atoms and the surface Si atoms. This trend, that had been observed already in previous DFT-LDA calculations [32,33], is confirmed in our present study.

IV. RESULTS AND DISCUSSION

Polarized RS spectra of the $(\sqrt{3} \times \sqrt{3})$ Pb/Si(111) surface are shown in Fig. 2 for the $\mathbf{z}(\mathbf{y}\mathbf{y})\bar{\mathbf{z}}$ (A' symmetry) and the $\mathbf{z}(\mathbf{x}\mathbf{y})\bar{\mathbf{z}}$ (A'' symmetry) polarization configurations. The surface vibrational contributions (surface Raman spectra) are clearly evident in the difference of spectra recorded on the clean reconstructed and the disordered reference surface. Comparison of the clean and disordered reference surface reveals the structured surface Raman spectrum superimposed on a smooth background. Differences related to the polarization configuration, e.g., mode symmetries, are only weakly pronounced.

To further evaluate the surface vibrational properties, the surface Raman spectra for both polarization configurations

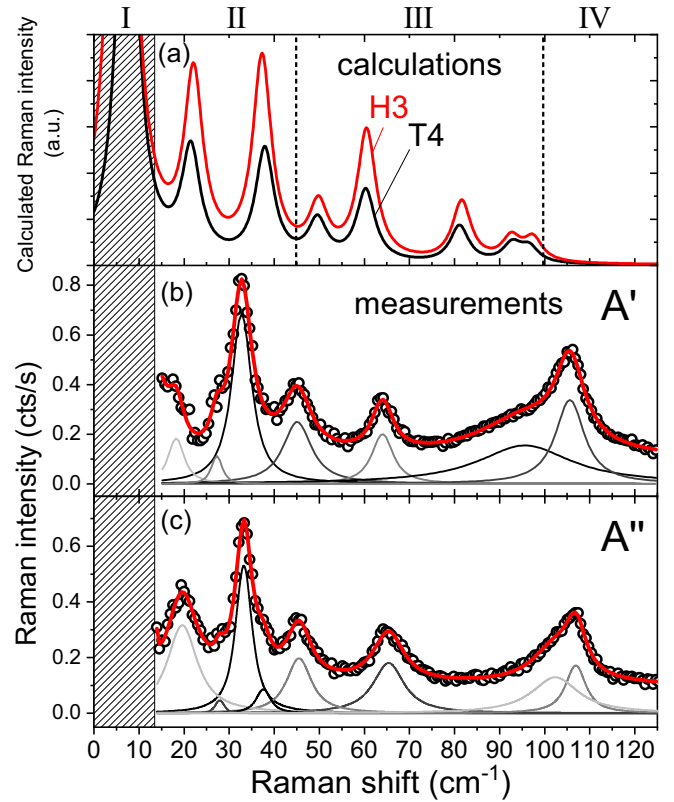


FIG. 3. Low energy Raman spectra of the $(\sqrt{3} \times \sqrt{3})$ reconstruction in A' and A'' symmetries in comparison to calculated Raman spectra from phonon modes at the Brillouin zone center of both the T4 and H3 structures. The calculated spectrum consists of Lorentzian peaks broadened by 5 cm^{-1} . The calculated vibrational eigenfrequencies of T4 and H3 zone center modes are listed in Table I. Measured spectra [open circles in (b) and (c)] are fitted by Voigt line profiles and the according peak positions also listed in Table I.

have been analyzed by curve fitting with Voigt line profiles after background subtraction (Fig. 3). The curve fitting is restricted to peaks which significantly exceed the noise level. According frequencies and linewidths are given in Table I. The surface Raman modes are observed in both scattering configurations, but with different Raman intensities, in A' and A'' mode symmetries. This finding substantiates clearly the assignment of the Raman lines to surface vibrational eigenmodes, but a clear identification of mode symmetry is not possible.

In the case of an ordered surface structure only the zone center modes show up in the surface Raman spectra [19,20]. Thus in the following we will discuss the experimental surface Raman spectra with respect to calculated zone center modes for both the H3 and T4 structures (as shown in Fig. 3).

Despite the very different alignment of the Pb layer with respect to the Si substrate in H3 and T4 structural models (Fig. 1), the according calculated vibrational spectra are very similar [Fig. 3(a)]. This suggests, supported also by the comparably large distance of the Pb layer to the first Si layer [(side view on top of Fig. 1)], a high degree of decoupling between the Pb layer and the Si substrate. Each contains a

TABLE I. Compilation of calculated Γ -point vibrations in T4 and H3 structures and measured A' and A'' modes. The FWHM of measured lines is indicated in parenthesis. The confidence interval of frequency positions ($<0.5 \text{ cm}^{-1}$) is well below the specified linewidths.

Mode class	T4 (cm^{-1})	H3 (cm^{-1})	Expt. A' (cm^{-1})	Expt. A'' (cm^{-1})
(I)				
in plane	7.1	5.9		
sliding	7.7	6.5		
(II)				
mixed	21.5	22.1	18.2 (4.8)	19.6 (9.6)
out-of-plane	37.9	37.3	32.8 (6.3)	33.2 (4.8)
(III)				
in plane	49.6	49.8	45.1 (9.2)	45.5 (7.8)
optical	60.3	60.5	64.0 (6.8)	65.4 (10)
	81.5	81.6		
	92.8	92.2	96 (>10)	102 (>10)
(IV)				
substrate				
surface			106 (>10)	107 (>10)
resonance				

largely independent set of vibrational modes confined within the Pb layer and the upper Si layers, respectively, which are weakly coupled by interatomic repulsion and/or electrostatic forces. Only in the modes below 15 cm^{-1} which are hardly accessible experimentally, the corrugated potential offered by the Si surface leads to noticeable changes in the vibrational frequencies of the Pb layer.

For the T4 structure a very complete picture including phonon dispersion, degree of surface localization, mode displacement patterns and density of phonon states is available from previous calculations (see Sec. III). The present calculations are extended to both H3 and T4 structures and are based on an improved approach with respect to that described in Ref. [23]. Nevertheless we find that the general results are still valid: Due to the large difference in atomic masses of Pb and Si, surface vibrations involving Pb displacements appear at low frequencies, while Si related vibrations appear at higher frequencies. Displacement patterns of the individual modes calculated in the present work based on the seven bilayer slab are shown in Figs. 4 and 5.

Based on these considerations we can classify the different types of surface vibrational modes for both H3 and T4 structural models (see also Table I):

(I) in-plane sliding vibrations of the whole Pb adlayer below 15 cm^{-1} ;

(II) out-of-plane vibrations with perpendicular displacements of the Pb adatoms in the range between $15\text{--}45 \text{ cm}^{-1}$;

(III) in-plane modes with combined displacements of both Si and Pb atoms between $45\text{--}95 \text{ cm}^{-1}$;

(IV) Si substrate related vibrations at higher frequencies, i.e., above 95 cm^{-1} .

Since the ground-state atomic structure slightly deviates from the C_{3v} symmetry, the modes appear in groups that result from a splitting of the degenerate modes (in the case

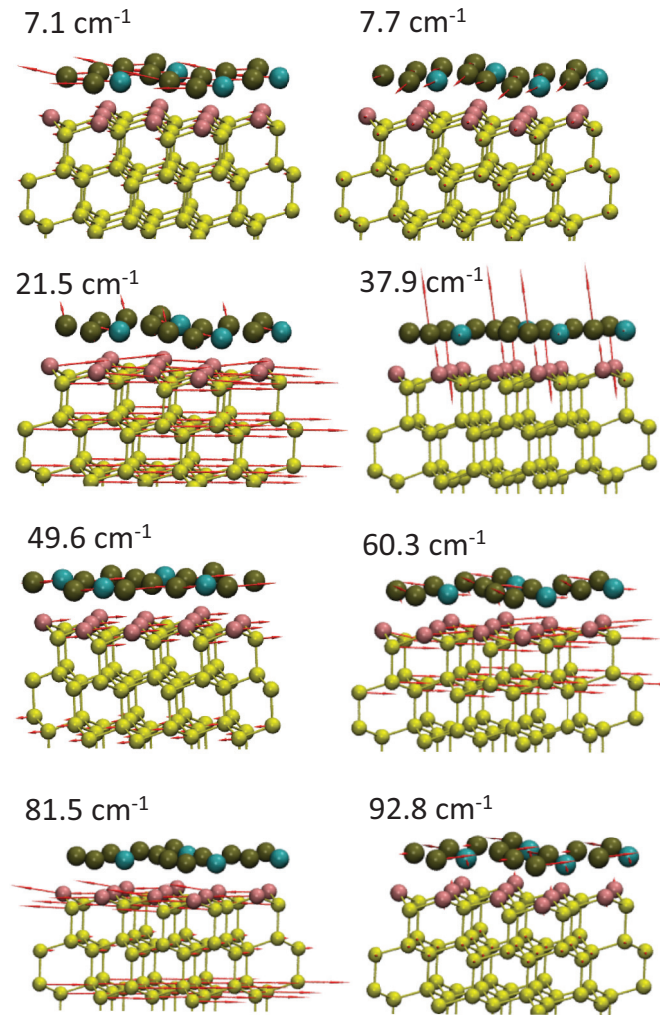


FIG. 4. Calculated vibrational patterns of the $(\sqrt{3} \times \sqrt{3})$ T4 reconstruction. The lengths of the arrows are proportional to the contribution of each atom to the eigenvector of the dynamical matrix. For the modes at 21.5 , 37.9 , and 60.3 cm^{-1} , one representative of three nearly degenerate eigenvectors is shown, while the modes at 49.6 , 81.5 , and 92.8 cm^{-1} are doubly degenerate.

of enforced symmetry). However, due to the small splitting ($<1 \text{ cm}^{-1}$) it is not resolved in the measurements. Moreover, we would like to note that the spectral range up to 15 cm^{-1} is not accessible by Raman spectroscopy due to filtering out the elastically scattered laser light. The low-frequency Raman peaks up to approximately 95 cm^{-1} are related to surface localized eigenmodes and are thus particularly dependent on the surface atomic structure, while the higher frequency modes are rather due to silicon substrate related vibrations.

Table I shows a compilation of experimentally determined Raman frequencies and linewidths together with the calculated modes (at Γ) for T4 and H3. We would like to note that both the A' and A'' modes are expected to be active in both the T4 and the H3 structures, albeit with different intensities. The displacement patterns of the respective modes are shown in Figs. 4 and 5 for the T4 and H3 structures, respectively.

In the range I of low frequency in-plane sliding vibrations, calculated for T4 and H3 ($7.1/7.7$ and $5.9/6.5 \text{ cm}^{-1}$,

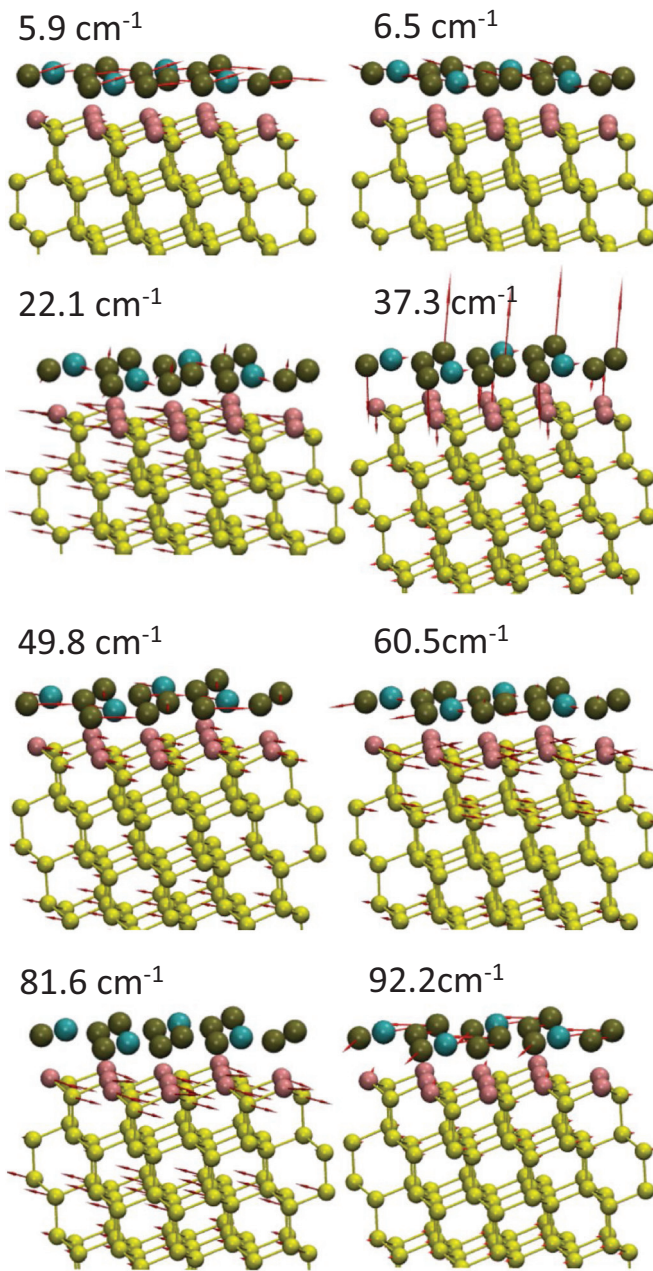


FIG. 5. Calculated vibrational patterns of the $(\sqrt{3} \times \sqrt{3})$ H3 reconstruction. For the modes at 22.1, 37.3, and 60.5 cm^{-1} , one representative of three nearly degenerate eigenvectors is shown, while the modes at 49.8, 81.6, and 92.2 cm^{-1} are doubly degenerate.

respectively), Raman lines cannot be observed experimentally due to stray light suppression. In the range II of out-of-plane vibrations with perpendicular displacements of the Pb adatoms, calculated surface modes arise at 21.5 and 37.9 for T4 and 22.1 and 37.3 cm^{-1} for H3. For H3, such out-of-plane modes have been reported at 26 and 41 cm^{-1} recently [27] which supports our present results. They refer to Raman lines at 18.2/19.6 cm^{-1} and 32.8/33.2 cm^{-1} found by curve fitting of the polarization resolved difference spectra. The linewidth of these modes varies between 4.8 and 9.6 cm^{-1} , which indicates that the broad peaks are most likely a superposition of several eigenmodes, as expected from calculations.

In the range III of in-plane modes with combined displacements of Si and Pb, calculated surface modes arise at 49.6 and 60.3 for T4 and 49.8 and 60.5 cm^{-1} for H3. They refer to Raman lines at 45.1/45.5 cm^{-1} , 64.0/65.4 cm^{-1} found by curve fitting of the polarization resolved difference spectra. The linewidth of these lines varies between 7 and 10 cm^{-1} , which indicates that they are also most likely a superposition of several eigenmodes. Moreover, calculated surface modes arise at 81.5 and 92.8 for T4 and at 81.6 and 92.2 cm^{-1} for H3. In the Raman spectra there appears a very broad band in the according spectral range which indicates the existence of surface modes but does not allow for a particular mode assignment.

In the range IV at frequencies higher than 95 cm^{-1} vibrational modes of the Si substrate layers occur which lead to very broad Raman bands. These modes are not well represented within the finite slab geometry applied in the calculations. However, these modes do not depend sensitively on the surface structure since they are not surface confined modes.

Altogether, the calculated H3 and T4 surface phonon modes give a very detailed interpretation of the experimentally observed surface Raman modes. Most of the calculated surface vibrational modes fit very well, i.e., within 3–5 cm^{-1} , to the Raman lines. Taking into account that the calculations are based on model structures which neglect the strain relief due to the coexistence of different domains in the SIC phase the agreement between experiment and theory is very satisfactory. The comparison between experiment and theory thus allows us to identify the type and even the atomic displacements of Pb/Si/111 surface modes. Only the two highest-energy surface optical modes around 81.5/81.6 cm^{-1} and 92.8/92.2 cm^{-1} cannot be resolved individually due to a very large linewidth in the respective Raman band.

In spite of the very good overall agreement between experiment and theory, however, it is impossible to distinguish between the two adsorption geometries H3 and T4 in the SIC phase, since the related calculated eigenmodes are much too close in eigenfrequency. The differences between experimental and calculated Raman spectra are larger than those between calculated H3 and T4 spectra.

As stated before, we conclude that the Pb adlayer is relatively weakly bound to the Si substrate, in accordance with the large binding distance between Pb and Si. Thus, the strong bonding within the Pb adlayer, on the one hand, and the structure of the uppermost few Si lattice planes, on the other hand, dominate the vibrational spectrum, while the difference in registry between T4 and H3 adlayers and the Si substrate yields only a small correction to mode frequencies. Moreover, we would like to point out that the Pb adlayer is not commensurate with the Si substrate, again in agreement with our view of a weakly bound adlayer structure and the finding of a very weak polarization dependence of Raman spectra.

The accuracy of the Raman calculations is limited on one hand due to the finite slab geometry and the assumption of nonresonant conditions. On the other hand the assignment of Raman lines to surface phonon modes at the Brillouin zone center is strictly correct only in ideally periodic structures. In the calculations, strain and grain boundaries (idealized model surface structures are used in the calculation) are neglected.

Modes with finite \mathbf{k} vectors may be activated in Raman scattering by the structural disorder, as realized for instance in a T4/H3 multidomain surface structure. However, as evident from the calculated dispersion relation [23,27], most of the surface localized modes employ rather flat dispersion branches. Thus it is justified to assume that the dominant part of the Raman signal of the surface confined modes is related to the Γ frequencies. Nevertheless, the line shape of the Raman lines, in particular, should carry additional information about domain size and domain distribution, similar as is known for nanocrystalline materials. This, on one hand, limits the present degree of agreement between Raman lines and calculated modes from the model structures, but on the other hand has the potential to extract more structural information with future capabilities.

V. SUMMARY

The vibrational properties of the SIC phase of Pb on Si(111) ($\sqrt{3} \times \sqrt{3}$) have been determined. Raman spectroscopy is used to detect surface vibrational Pb/Si interface modes representing unique experimental fingerprints of the atomic structure and chemical bonding. An overall assignment to microscopic surface modes has been achieved by comparison to respective *ab initio* calculations of the H3

and T4 adsorption geometries. The high similarity of surface phonons obtained in calculations for T4 and H3 atomic structures confirms a comparably high degree of decoupling of the Pb film with respect to the Si substrate. Pb-Pb interactions seem to play a more important role than Pb-Si bonds for structure formation of the Pb layer. We propose that the Raman spectrum may contain structural information on domain sizes and distributions which is not included in the present calculations. Thus, the knowledge acquired through SRS could be particularly valuable in future investigations of complex atomic surface structures such as, e.g., the linear phases of Pb/Si(111) in the *devil's staircase* regime or atomic Pb wires on the Si(557) surface [34].

ACKNOWLEDGMENTS

We gratefully acknowledge financial support by the Deutsche Forschungsgemeinschaft in the research unit FOR 1700, project ES 127/12-1 and within Collaborative Research Center SFB1242, project B02 at University Duisburg-Essen. Financial support by the Senatsverwaltung für Wirtschaft, Technologie und Forschung des Landes Berlin, the Ministerium für Innovation, Wissenschaft und Forschung des Landes Nordrhein-Westfalen, and the Bundesministerium für Bildung und Forschung is acknowledged.

-
- [1] P. C. Snijders and H. H. Weitering, *Rev. Mod. Phys.* **82**, 307 (2010).
- [2] R. W. Olesinski and G. J. Abbaschian, *Bull. Alloy Phase Diagrams* **5**, 271 (1984).
- [3] M. Zahedifar and P. Kratzer, *Phys. Rev. B* **96**, 115442 (2017).
- [4] K. Budde, E. Abraham, V. Yeh, and M. C. Tringides, *Phys. Rev. B* **61**, R10602(R) (2000).
- [5] S. Stepanovsky, M. Yakes, V. Yeh, M. Hupalo, and M. C. Tringides, *Surf. Sci.* **600**, 1417 (2006).
- [6] C. Tegenkamp, Z. Kallassy, H. Pfnür, H.-L. Günter, V. Zielasek, and M. Henzler, *Phys. Rev. Lett.* **95**, 176804 (2005).
- [7] J. H. Dil, F. Meier, J. Lobo-Checa, L. Patthey, G. Bihlmayer, and J. Osterwalder, *Phys. Rev. Lett.* **101**, 266802 (2008).
- [8] C. Tegenkamp, D. Lükermann, H. Pfnür, B. Slomski, G. Landolt, and J. H. Dil, *Phys. Rev. Lett.* **109**, 266401 (2012).
- [9] D. Eom, S. Qin, M.-Y. Chou, and C. K. Shih, *Phys. Rev. Lett.* **96**, 027005 (2006).
- [10] C. Brun, T. Cren, V. Cherkez, F. Debontridder, S. Pons, D. Fokin, M. C. Tringides, S. Bozhko, L. B. Ioffe, B. L. Altshuler, and D. Roditchev, *Nat. Phys.* **10**, 444 (2014).
- [11] T. Zhang, P. Cheng, W. J. Li, Y. J. Sun, G. Wang, X. G. Zhu, K. He, L. Wang, X. Ma, X. Chen, Y. Wang, Y. Liu, H. Q. Lin, J. F. Jia, and Q. K. Xue, *Nat. Phys.* **6**, 104 (2010).
- [12] M. Yakes, V. Yeh, M. Hupalo, and M. C. Tringides, *Phys. Rev. B* **69**, 224103 (2004).
- [13] L. Seehofer, G. Falkenberg, D. Daboul, and R. L. Johnson, *Phys. Rev. B* **51**, 13503 (1995).
- [14] T. L. Chan, C. Z. Wang, M. Hupalo, M. C. Tringides, Z. Y. Lu, and K. M. Ho, *Phys. Rev. B* **68**, 045410 (2003).
- [15] E. Ganz, H. Ing-Shouh, X. Fulin, S. K. Theiss, and J. Golovchenko, *Surf. Sci.* **257**, 259 (1991).
- [16] C. Kumpf, O. Bunk, J. H. Zeysing, M. M. Nielsen, M. Nielsen, R. L. Johnson, and R. Feidenhans'l, *Surf. Sci.* **448**, L213 (2000).
- [17] M. Svec, V. Chab, and M. C. Tringides, *J. Appl. Phys.* **106**, 053501 (2009).
- [18] X.-Y. Ren, H.-J. Kim, S. Yi, Y. Jia, and J.-H. Cho, *Phys. Rev. B* **94**, 075436 (2016).
- [19] N. Esser, *Appl. Phys. A* **69**, 507 (1999).
- [20] M. Liebhaber, U. Bass, P. Bayersdorfer, J. Geurts, E. Speiser, J. Räthel, A. Baumann, S. Chandola, and N. Esser, *Phys. Rev. B* **89**, 045313 (2014).
- [21] E. Speiser, N. Esser, S. Wippermann, and W. G. Schmidt, *Phys. Rev. B* **94**, 075417 (2016).
- [22] K. Fleischer, S. Chandola, N. Esser, W. Richter, and J. F. McGilp, *Phys. Rev. B* **67**, 235318 (2003).
- [23] S. Sakong, P. Kratzer, S. Wall, A. Kalus, and M. Horn-von Hoegen, *Phys. Rev. B* **88**, 115419 (2013).
- [24] J. P. Perdew, K. Burke, and M. Ernzerhof, *Phys. Rev. Lett.* **77**, 3865 (1996).
- [25] P. E. Blöchl, *Phys. Rev. B* **50**, 17953 (1994).
- [26] G. Kresse and J. Furthmüller, *Phys. Rev. B* **54**, 11169 (1996).
- [27] I. Yu. Sklyadneva, R. Heid, K.-P. Bohnen, P. M. Echenique, and E. V. Chulkov, *Phys. Rev. B* **97**, 195409 (2018).
- [28] M. Gajdoš, K. Hummer, G. Kresse, J. Furthmüller, and F. Bechstedt, *Phys. Rev. B* **73**, 045112 (2006).
- [29] P. Bruesch, *Phonons: Theory and Experiments II*, Springer Series Solid State Science, Vol. 65 (Berlin, 1986).
- [30] D. Karhánek, T. Bučko, and J. Hafner, *J. Phys.: Condens. Matter* **22**, 265006 (2010).
- [31] K. Fleischer, S. Chandola, N. Esser, W. Richter, and J. F. McGilp, *Phys. Rev. B* **76**, 205406 (2007).
- [32] J. Noffsinger and M. L. Cohen, *Solid State Commun.* **151**, 421 (2011).
- [33] G. Q. Huang, *New J. Phys.* **13**, 093023 (2011).
- [34] C. Tegenkamp, Z. Kallassy, H. L. Gunter, V. Zielasek, and H. Pfnür, *Euro. Phys. J. A* **43**, 557 (2005).